Frontiers of Information Technology & Electronic Engineering
www.jzus.zju.edu.cn; engineering.cae.cn; www.springerlink.com
ISSN 2095-9184 (print); ISSN 2095-9230 (online)
E-mail: jzus@zju.edu.cn

Motion detection for high-speed high-brightness objects based on a pulse array image sensor*

Peiwen ZHANG[1,2], Jiangtao XU‡[1,2], Huafeng NIE[1,2], Zhiyuan GAO[1,2], Kaiming NIE[1,2]

[1]*School of Microelectronics, Tianjin University, Tianjin 300072, China*

[2]*Tianjin Key Laboratory of Imaging and Sensing Microelectronic Technology, Tianjin 300072, China*

E-mail: neptune@tju.edu.cn; xujiangtao@tju.edu.cn; niehuafeng_ee@163.com; flyuphigher@outlook.com; nkaiming@tju.edu.cn

Received Aug. 11, 2020; Revision accepted May 16, 2021; Crosschecked Nov. 10, 2021

Abstract: We describe a method of optical flow extraction for high-speed high-brightness targets based on a pulse array image sensor (PAIS). PAIS is a retina-like image sensor with pixels triggered by light; it can convert light into a series of pulse intervals. This method can obtain optical flow from pulse data directly by accumulating continuous pulses. The triggered points can be used to filter redundant data when the target is brighter than the background. The method takes full advantage of the rapid response of PAIS to high-brightness targets. We applied this method to extract the optical flow of high-speed turntables with different background brightness, with the sensor model and actual data, respectively. Under the sampling condition of 2×10^4 frames/s, the optical flow could be extracted from a high-speed turntable rotating at 1000 r/min. More than 90% of redundant points could be filtered by our method. Experimental results showed that the optical flow extraction algorithm based on pulse data can extract the optical flow information of high-brightness objects efficiently without the need to reconstruct images.

Key words: Optical flow; Retina-like image sensor; Pulse triggered; High-speed targets; Vision processing
https://doi.org/10.1631/FITEE.2000407 **CLC number:** TP301.6

1 Introduction

Optical flow (OF) is a basic method in vision processing and has been widely used in various tasks, such as moving object detection (Pan JJ et al., 2018; Wang Z and Yang, 2018; Wang ZR et al., 2019), guiding the landing of an aircraft (Wang ZY et al., 2007), or extracting the shape of a moving object (Loucks et al., 1992; Zhang et al., 2015). Accurate and rapid extraction of OF and tracking of the target location are of great importance. However, due to occlusion, discontinuity, or non-ideal factors such as image sensor noise, OF extraction faces many difficulties. Although many efforts have been made to solve the problems and some results have been obtained, the extraction of OF is still challenging, especially when dealing with high-speed targets. The video sequence needed for OF extraction comes from image sensors, so the performance of image sensors has a great influence on the accuracy of OF extraction.

Traditional active pixel image sensors use frame scanning and multi-level quantization (Chae et al., 2010), and there are many methods to extract OF from videos captured by these image sensors (Fülöp and Zarándy, 2010; Pantilie and Nedevschi, 2010). These sensors and processing methods are suitable for low-speed applications. However, to capture high-speed targets, the frame frequency has to be increased. The direct consequence of increasing the frame frequency

‡ Corresponding author

* Project supported by the National Key R&D Program of China (No. 2019YFB2204202)

ORCID: Peiwen ZHANG, https://orcid.org/0000-0002-0040-8546; Jiangtao XU, https://orcid.org/0000-0003-1162-6562; Zhiyuan GAO, https://orcid.org/0000-0001-6708-6222; Kaiming NIE, https://orcid.org/0000-0002-5383-0580

is a linear increase in data volume. The huge amount of data brings not only the issues of transmission and storage, but also great challenges to machine vision processing, such as OF extraction and location tracking. Thus, traditional image sensors cannot deal with high-speed applications.

To reduce data volume and increase speed, dynamic vision sensors (DVSs) based on the human retina have been proposed (Lichtsteiner et al., 2008; Posch et al., 2009; Moeys et al., 2018; Suh et al., 2020). In contrast to traditional image sensors that capture images using a shutter, each pixel in DVS works independently, reporting changes in brightness as events. The events and address of the pixel compose the asynchronous address-event representation (AER) in DVSs. A DVS indicates positive and negative changes in light intensity at each pixel address, generating ON and OFF events, respectively. The sparse address event output reduces the memory requirement and computational cost, which makes DVS applicable to high-speed low-power applications. In view of the great difference between the outputs of AER and traditional image sensors, Benosman et al. (2012) first proposed a process to compute OF using an asynchronous-event-based retina at high speed and with low computational load. This work showed that the current limitations of OF computation could be overcome by using event-based visual acquisition, in which high data sparseness and high temporal resolution permit the computation of OF with micro-second accuracy and at very low computational cost. Benosman et al. (2014) introduced a framework to estimate visual flow from the local properties of the spatio-temporal space of events. Through turntable experiments, they determined the limit speed of DVS to extract the OF of a high-speed target. Limited by data throughput, DVS cannot obtain accurate OF when the turntable speed is greater than 2000 r/min. However, AER sensors have great disadvantages in image restoration and data integrity. Berner et al. (2013) developed the dynamic and active-pixel vision sensor (DAVIS) structure, which combines DVS and active-pixel sensor (APS) output image information and event information. However, because the temporal resolutions of the DVS and APS data cannot match, it is difficult to apply the event information to the image restoration of APS.

To solve these problems, a pulse array image sensor (PAIS) using pulse interval representation was proposed in our previous work (Gao et al., 2018). In principle, it is similar to pulse frequency modulation, which outputs a series of 1-bit data to express light intensity. This sensor scans at a high frame rate while retaining a small amount of data. Compared with traditional image sensors, PAIS has a lower data volume and higher time resolution. Compared with AER image sensors, it has higher data completeness and overcomes the limitations of AER sensors in motion detection in high-speed environments. Based on PAIS, we propose an OF extraction algorithm for high-speed high-brightness targets using pulse interval events. In many high-speed scenes, the algorithms used, such as particle image velocimetry (PIV) (Brooks et al., 2018) and cloud droplet probe (CDP) (Lance et al., 2010), pay more attention to the motion of highlighted objects in a dark background. In contrast, our algorithm uses an event selection filter formed naturally by the sensor to reduce the computational cost of OF extraction.

2 Sensor structure and pixel working principle

Fig. 1 shows a structure diagram of PAIS. It consists of a pulse pixel array, row and column driving circuit, timing control and latching circuit, reference voltage and current generation circuit, low-voltage differential signaling (LVDS) interface circuit, and serial peripheral interface (SPI) circuit. The image sensor uses pulse intervals to express light intensity information, which can reduce the data rate effectively. It uses high-speed readout timing to achieve high time resolution and detect high-speed objects promptly and effectively, and an asynchronous reset to ensure that the pixel units can detect scene information continuously and integrally. The image sensor communicates with an external microcontroller through an SPI. It can modify the main parameters such as clock frequency, reference voltage, and reset voltage. Pulse data is outputted by 10 high-speed LVDS interfaces through the readout circuit.

The pixel unit converts the optical signal into an electrical signal and accumulates photocurrent. When the accumulation exceeds a preset threshold, the pixel

will be triggered to output a pulse signal, and at the same time be reset immediately to restart the exposure of a new cycle, and the pulse signal will be maintained until the reading period arrives. The pixel structure and working principle are shown in Fig. 2. The pixel unit is composed mainly of a pulse generation unit, self-reset unit, and readout circuit unit. In the pulse generation stage, the photodiode converts the photocurrent I_{ph} into a voltage signal V_{pix}. With the continuous input of photons, the voltage at V_{pix} decreases continuously. When it reaches the threshold of reference voltage V_{ref}, the comparator flips to generate a pulse. When the reset unit receives the pulse signal, a photodiode reset signal is generated immediately. After a short fixed delay, the pixel unit starts to accumulate photocurrent again. The readout circuit unit stores the pulse data, which is read by high-speed scanning at the time shown by each dashed line in Fig. 3.

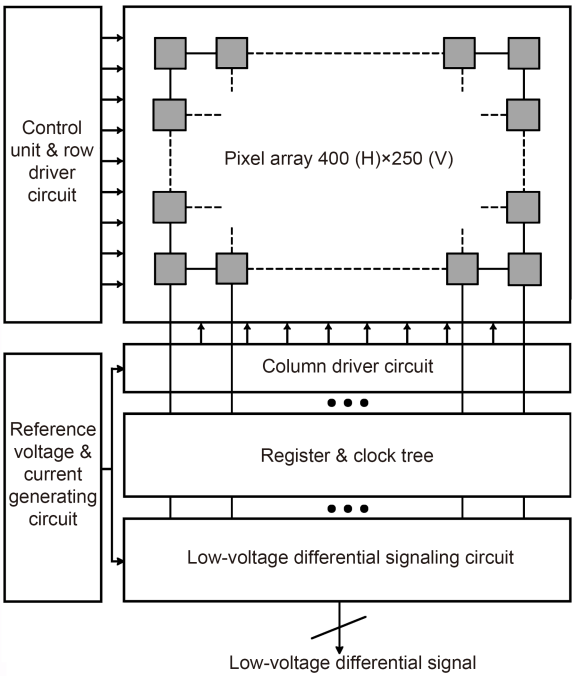

Fig. 1 Modular structure of the pulse array image sensor

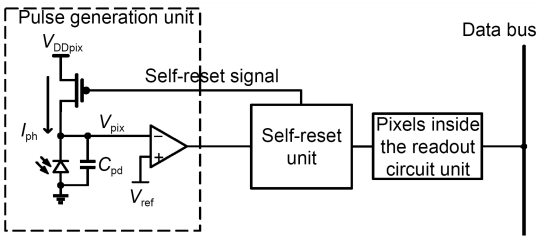

Fig. 2 Pulse pixel unit structure

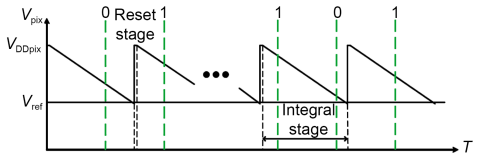

Fig. 3 Pulse pixel trigger sequence diagram

Based on the pixel's working principle, the photocurrent I_{ph} is inversely proportional to the exposure time interval t of the pixel. The formula can be expressed as follows:

$$t = \frac{C_{pd}(V_{DDpix} - V_{ref})}{I_{ph}}, \tag{1}$$

where C_{pd} is the capacitance of the photodiode and V_{DDpix} is the voltage of the power supply.

3 Optical flow based on pulse data

OF algorithms have been described in detail many times in previous papers (Barron et al., 1994; Denman et al., 2009, 2010; Pan YJ et al., 2020). After the appearance of DVS and DAVIS, OF methods have been widely studied (Benosman et al., 2012; Brosch et al., 2015; Rueckauer and Delbruck, 2016; Ridwan and Cheng, 2017; Valeiras et al., 2019; Zhu et al., 2019; Almatrafi and Hirakawa, 2020; Low et al., 2020). The OF extraction method based on PAIS is different from those based on traditional image sensors and DVSs. PAIS generates discrete pulses instead of grayscale or events. The pulse flow diagram of an actual turntable is shown in Fig. 4. A surface of pulse can be obtained at each readout time. The basic assumption of OF is that the gray level of a moving object remains unchanged within a short interval of time.

$$I(x,y,t) = I(x + \delta x, y + \delta y, t + \delta t), \tag{2}$$

where I is the grayscale function of the input picture. By introducing all smooth constraints, the vector value of the OF field (u, v) can be obtained.

$$I_x u + I_y v + I_t = 0. \tag{3}$$

Eq. (3) shows that spatial and temporal derivatives are needed in traditional OF methods. These derivatives exist naturally in traditional sensors based

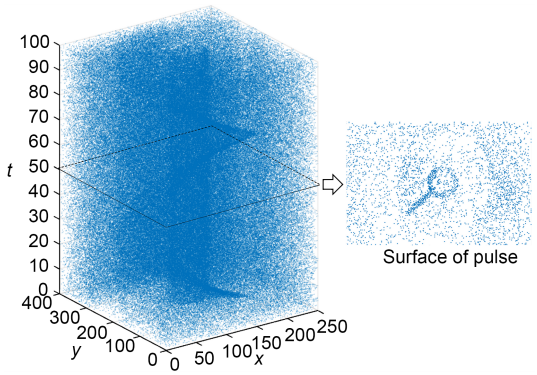

Fig. 4 Pulse flow diagram and surface of pulse of the turntable

on grayscale and frames. However, the output data of PAIS contains only discrete 1-bit sequences of "0" and "1," without gray levels (Eq. (2)). The absence of gray levels makes it difficult to compute spatial and temporal gradients in Eq. (3). To represent the spatial derivatives, we accumulate the continuous pulse data over a period of time to substitute for the gray value information. Suppose E is the equivalent intensity of I for PAIS. f is the time for calculating the accumulated pulse. P is the number of successive pulse frames extracted in a specific time decided by f. f, f_1, and f_2 are three different times. In general, $20>f_2-f>2$, $f_2>f_1>f$. The temporal derivative is represented by the accumulated pulse difference of adjacent points in different periods. The spatial and temporal derivatives can be substituted by

$$\begin{cases} \dfrac{\mathrm{d}E(x,y,f)}{\mathrm{d}x} = \\ \quad \sum_{f-f_2}P(x+1,y+1)+\sum_{f-f_2}P(x+1,y) \\ \quad -\sum_{f-f_2}P(x,y+1)-\sum_{f-f_2}P(x,y), \\ \dfrac{\mathrm{d}E(x,y,f)}{\mathrm{d}y} = \\ \quad \sum_{f-f_2}P(x+1,y+1)+\sum_{f-f_2}P(x,y+1) \\ \quad -\sum_{f-f_2}P(x+1,y)-\sum_{f-f_2}P(x,y), \\ \dfrac{\mathrm{d}E(x,y,f)}{\mathrm{d}t} = \\ \quad \sum_{f-f_1}P(x+1,y+1)+\sum_{f-f_1}P(x+1,y) \\ \quad +\sum_{f-f_1}P(x,y+1)+\sum_{f-f_1}P(x,y) \\ \quad -\sum_{f_1-f_2}P(x+1,y+1)-\sum_{f_1-f_2}P(x+1,y) \\ \quad -\sum_{f_1-f_2}P(x,y+1)-\sum_{f_1-f_2}P(x,y). \end{cases} \tag{4}$$

The OF vector (u, v) can be solved by replacing Eq. (4) with the OF constraint equation, Eq. (3). In this way the OF can be extracted without reconstructing the grayscale images. We compute only the OF of triggered points instead of dense OF to reduce the computational cost. When the targets of interest are brighter than the background, the triggered points can be used as an event selection filter to wipe out most redundant points, because pulses are dense in bright areas. A flow chart of the method is shown in Fig. 5.

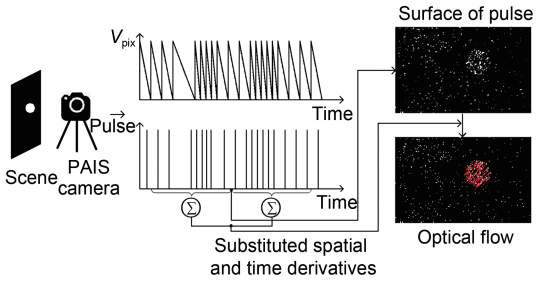

Fig. 5 Flow chart of the optical flow extraction method

4 Experiments and results

4.1 Optical flow in the PAIS model

The image reconstruction method and behavior-level model of the image sensor were established in our previous study (Xu et al., 2019). We used the model to simulate a high-speed revolving turntable. The rotation speed was simulated as 1000 r/min. The input of the model was a synthetic video of a revolving turntable with adjustable brightness. The output videos were made up of pulse interval reconstructed frames. Here, the reset voltage V_{DDpix} of the behavior-level model was set as 3.0 V, the reference voltage V_{ref} as 2.0 V, and the frame cycle as 50 μs.

Supposing that the bright bar was the object area of interest, we simulated the OF extraction of the turntable with different gray levels of background. The reconstructed images, the OF, and the triggered points are shown in Fig. 6. The results of OF calculation are marked with arrows on the input picture of the first frame. The direction of the arrow represents the direction of the OF vector. The length of the arrow represents the length of the vector: the longer the arrow, the higher the speed. The triggered points in

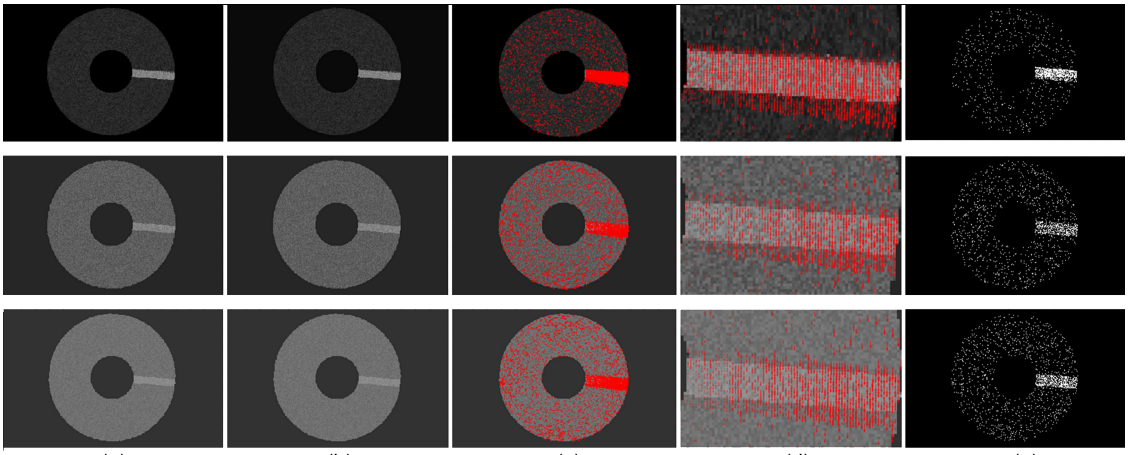

Fig. 6 Optical flow extraction of a synthetic turntable with different brightness: (a) frame 1; (b) frame 11; (c) optical flow vector extraction results; (d) details of the enlarged image of (c); (e) triggered point distribution

The top, middle, and bottom rows represent the turntables with background brightness of 50, 80, and 100 lux, respectively

Fig. 6e are indicated by bright spots. Because of the long trigger interval of the pixels in the dark background and the short trigger time of the pixels in a bright target, the OF calculation results are all concentrated in the bright target area, which greatly improves the calculation efficiency and accuracy.

The grayscale images in Fig. 6 were reconstructed by the pulse interval restoration method. These images can make the optical extraction result intuitive. Based on the working mode of the pixel, the output of the PAIS is known to be a single bit of pulse data. To make people intuitively observe the environmental information captured by the sensor, it is necessary to convert the pulse data into light intensity information. Based on the sensor model, the relationship between the different pulse data and the light intensity information was analyzed in detail. The pulse interval is inversely proportional to the intensity of light. There are two methods to reconstruct frames, namely pulse cumulative restoration and pulse interval restoration. The pulse interval restoration method is more suitable for obtaining clear images of high-speed objects. The OF can be extracted from the pulse data directly without reconstructing the grayscale images.

Table 1 shows the OF extraction results of the PAIS model with different simulated relative turntale background brightness. The total number of triggered points and the number of points in the bright target area are listed. The total filtration ratio is the proportion of the number of non-triggered points to that of total pixels. The point ratio in the target area is the proportion of the number of triggered points in the bright target area to that of the total triggered points. The average end-point error (AEE) and average angular error (AAE) were used to assess the accuracy of OF extraction (Rueckauer and Delbruck, 2016). The data in Table 1 is presented in Fig. 7. The results showed that as the background became brighter, the total number of triggered points increased, so the total filtration ratio decreased, which means that the amount of

Table 1 Results for optical extraction of the PAIS model

Background brightness (lux)	Point number		Ratio (%)		AEE (%)	AAE (°)
	Total triggered	In the target area	Total filtration ratio	In the target area		
50	2017	715	97.98	35.45	23.29±9.89	0.89±0.42
60	2124	697	97.88	32.82	15.90±7.87	0.58±0.31
70	2249	614	97.75	27.30	24.73±7.45	0.94±0.62
80	2291	597	97.71	26.06	19.34±7.27	0.82±0.53
90	2533	573	97.47	22.62	25.33±8.30	0.93±0.59
100	2719	516	97.28	18.98	37.97±9.39	1.61±0.51

AEE: average end-point error; AAE: average angular error

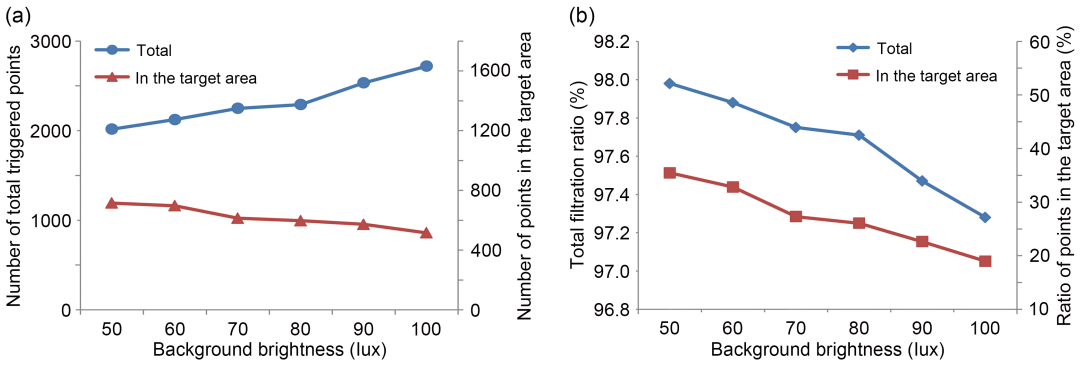

Fig. 7 Trigger conditions under different background brightness: (a) number of total triggered points and points in the target area; (b) total filtration ratio and ratio of triggered points in the target area

calculation increased. The number of points and the point ratio in the target area decreased, which means that the amount of effective calculation decreased. The experimental results showed that the darker the background of the turntable, the higher the filtration ratio, and the more concentrated are the triggered points in the bright target area. This shows that the efficiency of OF extraction is higher in the case of a dark background. The AEE value was small and fluctuated little, indicating that the OF accuracy is not obviously affected by the background brightness.

4.2 Real optical flow extraction

In this study, a testing system was built using a sensor camera designed by our team. A physical picture of the camera is shown in Fig. 8. The sensor transmits data to the collector by driving the printed circuit board (PCB). The collector transmits the sensor pulse data to the computer through the USB3.0 serial port and saves it. The sensor takes pictures at a frame rate of 2×10^4 frames/s. The data volume is 250×400×20 000 bits/s, which can be restored to the corresponding 2×10^4 frames/s high-speed video sequence by post-processing.

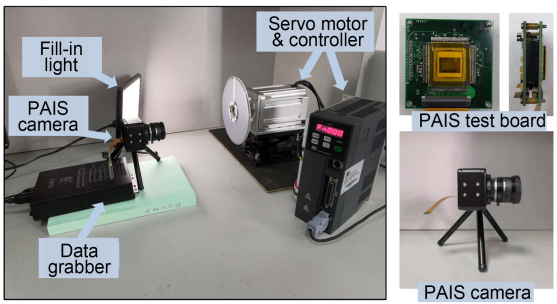

Fig. 8 PAIS camera and imaging system

We made three turntables with different background gray levels and photographed the images at a speed of 1000 r/min. We also made a moving ball to show the translation and scaling situations (Fig. 9). To test the influence of speed on OF extraction, an experiment using a turntable in medium background brightness at different speeds was carried out (Fig. 10). The ground truth was estimated by the turntable's rotating speed and the ball's geometric center.

Fig. 9 shows that the triggered points were concentrated in the bright area. The PAIS had 250×400 pixels. If all OF calculations were carried out, a lot of invalid time would be consumed. Although the real experiment was affected by noise, uneven illumination, metal device reflection, and other adverse factors, most redundant untouched pixels were filtered through triggered points. As shown in Table 2, this method can effectively filter more than 90% of the pixels. The operation efficiency was greatly improved.

The experimental results showed that the efficiency of OF extraction using a dark background was higher. In practice, because the trigger time of the pixel is determined by the reset voltage and the reference voltage, high-efficiency OF target extraction can be achieved by adjusting the reset voltage and the reference voltage of the PAIS to an appropriate level. The efficiency of OF extraction is high when the difference in brightness between a bright object and a dark background is large. Table 3 shows that the speed factor had little effect on the extraction result when the rotating speed was less than 3500 r/min. When the rotating speed was too high, the pulse data smeared and attenuated OF extraction.

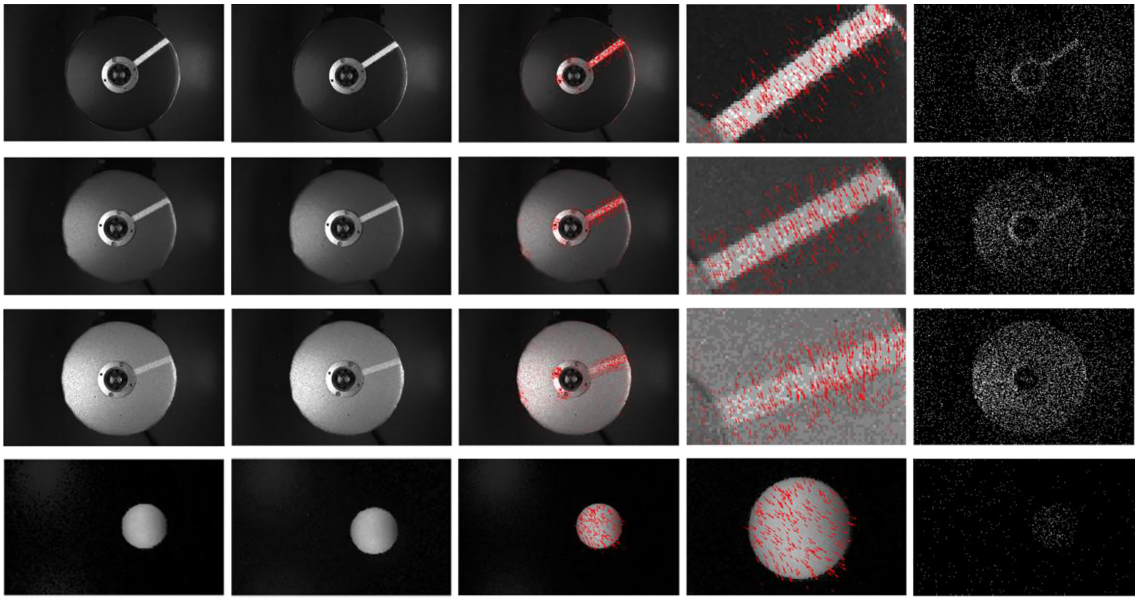

Fig. 9 Optical flow extraction of a real turntable with different brightness: (a) frame 1; (b) frame 11; (c) optical flow vector extraction results; (d) details of the enlarged image of (c); (e) triggered point distribution

The first, second, and third rows represent the turntable with low, medium, and high background brightness, respectively; the last row represents a ball moving towards the camera

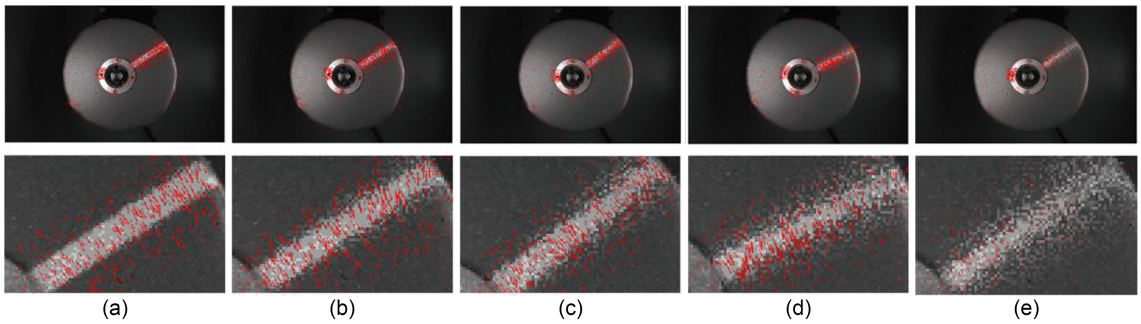

Fig. 10 Optical flow extraction of a real turntable at a rotating speed of 500 (a), 1500 (b), 2000 (c), 3000 (d), and 4000 (e) r/min

First row: optical flow vector extraction results; second row: details of the enlarged images

Table 2 Results for optical extraction from a real PAIS camera

Background brightness (lux)	Point number		Ratio (%)		AEE (%)	AAE (°)
	Total triggered	In the target area	Total filtration ratio	In the target area		
Low	4328	198	95.67	4.57	31.38±5.55	6.44±1.51
Medium	5320	159	94.68	2.99	55.19±3.96	1.71±2.94
High	7836	140	92.16	1.79	58.23±2.71	18.64±1.72
Moving ball	545	217	99.45	39.82	78.19±2.78	5.74±1.26

AEE: average end-point error; AAE: average angular error

4.3 Comparisons with other methods

Comparative experiments were performed using the jAER dataset (Rueckauer and Delbruck, 2016). This dataset obtains the ground truth speed from the inertial measurement unit (IMU). This dataset contains sequences of translation and rotation. We obtained pulse data from the PAIS behavior-level model (Xu et al., 2019), as shown in Fig. 11, and assessed the data using the APS method (Sun et al., 2010) and DVS methods (Benosman et al., 2014; Rueckauer

Table 3 Results of optical extraction from a real PAIS camera at different speeds

Rotating speed (r/min)	Point number		Ratio (%)		AEE (%)	AAE (°)
	Total triggered	In the target area	Total filtration ratio	In the target area		
500	5371	163	94.63	3.03	44.16±2.68	10.51±3.11
1000	5385	138	94.61	2.56	51.09±3.40	15.01±1.96
1500	5352	108	94.65	2.02	51.76±3.60	15.20±1.73
2000	5316	97	94.68	1.82	48.50±4.09	12.46±1.54
2500	5390	105	94.61	1.95	50.26±2.06	12.30±0.95
3000	5499	90	94.50	1.64	41.07±2.19	10.31±2.63
3500	5480	88	94.52	1.61	58.81±3.23	18.72±2.50
4000	5478	57	94.52	1.04	71.01±9.59	30.34±3.89
4500	5327	71	94.67	1.33	72.81±7.43	39.36±4.05

AEE: average end-point error; AAE: average angular error

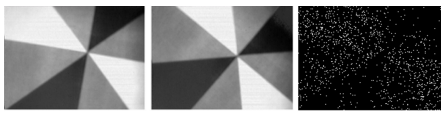

Fig. 11 Intensity image frames of the rotating disk sequence (a) and the surface of pulse from the PAIS behavior-level model (b)

and Delbruck, 2016; Zhu et al., 2018). The results are shown in Fig. 12 and Table 4.

It can be seen that our method could perform as well as the state-of-the-art methods. The APS method performed better because an APS camera collects the brightness of every point and has the largest amount of

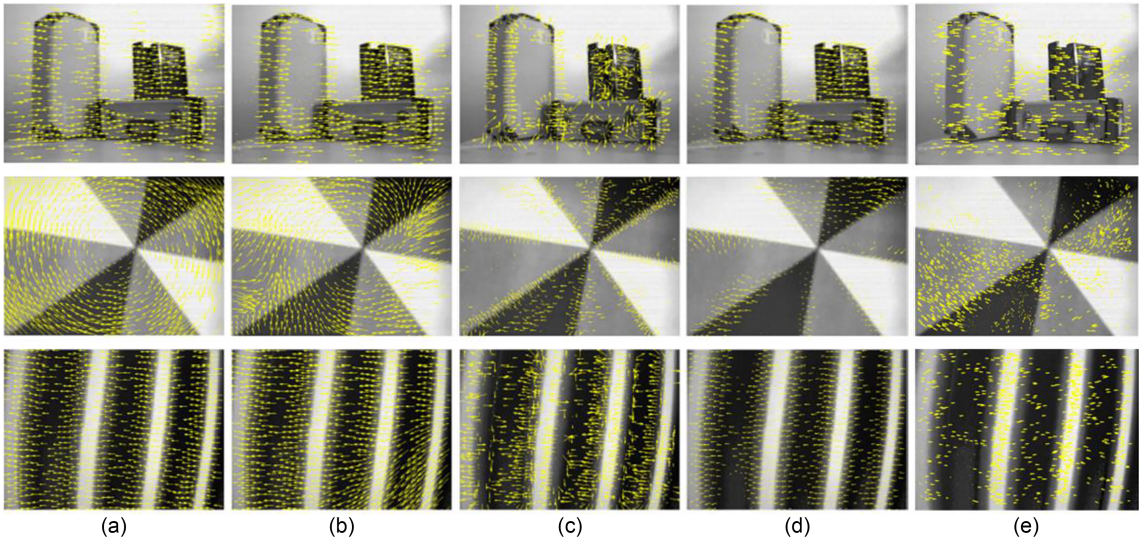

Fig. 12 Optical flow extraction results: (a) ground truth; (b) APS-OF method Classical$_{++}$; (c) DVS-OF method LK$_{CD1}$; (d) DVS-OF method EV-FlowNet; (e) PAIS-OF method

First row: translating box sequences; second row: rotating disk sequences; third row: translating sinusoidal pattern sequences

Table 4 AEE and AAE of APS, DVS, and PAIS optical flow methods

Data type	Method	AEE (%)			AAE (°)		
		Translating box	Rotating disk	Translating sinusoidal	Translating box	Rotating disk	Translating sinusoidal
APS	Classical$_{++}$*	17.15±10.21	27.58±20.04	32.72±19.97	2.09±3.60	10.76±10.79	5.25±7.63
DVS	LK$_{CD1}$**	58.13±28.86	54.46±34.89	57.16±25.55	28.98±31.27	19.93±21.35	21.72±35.31
	EV-FlowNet***	29.28±17.97	99.46±73.50	56.97±23.30	7.21±10.80	36.00±30.57	6.20±5.13
PAIS	Our method	32.36±19.31	47.42±35.09	51.24±22.07	12.54±5.28	23.42±20.65	17.36±13.27

*Sun et al., 2010. **Benosman et al., 2014; Rueckauer and Delbruck, 2016. ***Zhu et al., 2018

AEE: average end-point error; AAE: average angular error

data. Both APS and DVS methods compute dense OF. Our method computes unevenly distributed sparse OF and concentrates on the bright area, leading to a lower computation cost. It has a natural advantage when the targets are bright objects.

5 Conclusions

In this study, we proposed an alternative framework to calculate OF based on PAIS. This sensor represents light intensity information with pulse intervals. The OF extraction method makes full use of the advantages of the PAIS. Experiments showed that the OF extraction method can filter the redundant information efficiently for high-speed high-brightness targets. The results presented should be valuable in applications requiring rapid and even real-time analysis of high-speed events, such as vision-based guidance for imaging moving projectiles or high-speed autonomous aircraft.

Contributors

Peiwen ZHANG and Huafeng NIE designed the research. Jiangtao XU pointed out the key research directions. Peiwen ZHANG drafted the paper. Zhiyuan GAO and Kaiming NIE helped organize the paper and ensure its quality. Peiwen ZHANG and Jiangtao XU revised and finalized the paper.

Compliance with ethics guidelines

Peiwen ZHANG, Jiangtao XU, Huafeng NIE, Zhiyuan GAO, and Kaiming NIE declare that they have no conflict of interest.

References

Almatrafi M, Hirakawa K, 2020. DAViS camera optical flow. *IEEE Trans Comput Imag*, 6:396-407. https://doi.org/10.1109/TCI.2019.2948787

Barron JL, Fleet DJ, Beauchemin SS, 1994. Performance of optical flow techniques. *Int J Comput Vis*, 12(1):43-77. https://doi.org/10.1007/bf01420984

Benosman R, Ieng SH, Clercq C, et al., 2012. Asynchronous frameless event-based optical flow. *Neur Netw*, 27:32-37. https://doi.org/10.1016/j.neunet.2011.11.001

Benosman R, Clercq C, Lagorce X, et al., 2014. Event-based visual flow. *IEEE Trans Neur Netw Learn Syst*, 25(2): 407-417. https://doi.org/10.1109/tnnls.2013.2273537

Berner R, Brandli C, Yang MH, et al., 2013. A 240×180 120dB 10mW 12μs-latency sparse output vision sensor for mobile applications. Symp on VLSI Circuits, p.C186-C187. https://doi.org/10.5167/uzh-91116

Brooks JM, Gupta AK, Smith MS, et al., 2018. Particle image velocimetry measurements of Mach 3 turbulent boundary layers at low Reynolds numbers. *Exp Fluids*, 59(5):83. https://doi.org/10.1007/s00348-018-2536-x

Brosch T, Tschechne S, Neumann H, 2015. On event-based optical flow detection. *Front Neurosci*, 9:137. https://doi.org/10.3389/fnins.2015.00137

Chae Y, Cheon J, Lim S, et al., 2010. A 2.1Mpixel 120frame/s CMOS image sensor with column-parallel ΔΣ ADC architecture. IEEE Int Solid-State Circuits Conf, p.394-395. https://doi.org/10.1109/ISSCC.2010.5433974

Denman S, Fookes C, Sridharan S, 2009. Improved simultaneous computation of motion detection and optical flow for object tracking. Proc Digital Image Computing: Techniques and Applications, p.175-182. https://doi.org/10.1109/DICTA.2009.35

Denman S, Fookes C, Sridharan S, 2010. Group segmentation during object tracking using optical flow discontinuities. 4th Pacific-Rim Symp on Image and Video Technology, p.270-275. https://doi.org/10.1109/PSIVT.2010.52

Fülöp T, Zarándy Á, 2010. Bio-inspired looming object detector algorithm on the Eye-RIS focal plane-processor system. 12th Int Workshop on Cellular Nanoscale Networks and Their Applications, p.1-5. https://doi.org/10.1109/CNNA.2010.5430290

Gao J, Wang YZ, Nie KM, et al., 2018. The analysis and suppressing of non-uniformity in a high-speed spike-based image sensor. *Sensors*, 18(12):4232. https://doi.org/10.3390/s18124232

Lance S, Brock CA, Rogers D, et al., 2010. Water droplet calibration of the cloud droplet probe (CDP) and in-flight performance in liquid, ice and mixed-phase clouds during ARCPAC. *Atmos Meas Techn*, 3(6):1683-1706. https://doi.org/10.5194/amt-3-1683-2010

Lichtsteiner P, Posch C, Delbruck T, 2008. A 128×128 120 dB 15 μs latency asynchronous temporal contrast vision sensor. *IEEE J Sol-State Circ*, 43(2):566-576. https://doi.org/10.1109/JSSC.2007.914337

Loucks T, Ghosh BK, Lund J, 1992. An optical flow based approach for motion and shape parameter estimation in computer vision. Proc 31st IEEE Conf on Decision and Control, p.819-823. https://doi.org/10.1109/CDC.1992.371611

Low WF, Gao Z, Xiang C, et al., 2020. SOFEA: a non-iterative and robust optical flow estimation algorithm for dynamic vision sensors. IEEE/CVF Conf on Computer Vision and Pattern Recognition Workshops, p.368-377. https://doi.org/10.1109/CVPRW50498.2020.00049

Moeys DP, Corradi F, Li C, et al., 2018. A sensitive dynamic and active pixel vision sensor for color or neural imaging applications. *IEEE Trans Biomed Circ Syst*, 12(1):123-136. https://doi.org/10.1109/TBCAS.2017.2759783

Pan JJ, Tian Y, Zhang X, et al., 2018. Infrared target detection based on local contrast method and LK optical flow. IEEE 3rd Optoelectronics Global Conf, p.176-179. https://doi.org/10.1109/OGC.2018.8529967

Pan YJ, Sun XY, Wu F, 2020. Enriching optical flow with appearance information for action recognition. IEEE Int Conf on Visual Communications and Image Processing, p.251-254.

https://doi.org/10.1109/VCIP49819.2020.9301827

Pantilie CD, Nedevschi S, 2010. Real-time obstacle detection in complex scenarios using dense stereo vision and optical flow. Proc 13th Int IEEE Conf on Intelligent Transportation Systems, p.439-444. https://doi.org/10.1109/ITSC.2010.5625174

Posch C, Matolin D, Wohlgenannt R, et al., 2009. A microbolometer asynchronous dynamic vision sensor for LWIR. *IEEE Sens J*, 9(6):654-664. https://doi.org/10.1109/JSEN.2009.2020658

Ridwan I, Cheng H, 2017. An event-based optical flow algorithm for dynamic vision sensors. In: Karray F, Campilho A, Cheriet F (Eds.), Image Analysis and Recognition. Springer, Cham, p.182-189. https://doi.org/10.1007/978-3-319-59876-5_21

Rueckauer B, Delbruck T, 2016. Evaluation of event-based algorithms for optical flow with ground-truth from inertial measurement sensor. *Front Neurosci*, 10:176. https://doi.org/10.3389/fnins.2016.00176

Suh Y, Choi S, Ito M, et al., 2020. A 1280×960 dynamic vision sensor with a 4.95-μm pixel pitch and motion artifact minimization. IEEE Int Symp on Circuits and Systems, p.1-5. https://doi.org/10.1109/ISCAS45731.2020.9180436

Sun DQ, Roth S, Black MJ, 2010. Secrets of optical flow estimation and their principles. IEEE Computer Society Conf on Computer Vision and Pattern Recognition, p.2432-2439. https://doi.org/10.1109/CVPR.2010.5539939

Valeiras DR, Clady X, Ieng SH, et al., 2019. Event-based line fitting and segment detection using a neuromorphic visual sensor. *IEEE Trans Neur Netw Learn Syst*, 30(4): 1218-1230. https://doi.org/10.1109/TNNLS.2018.2807983

Wang Z, Yang XJ, 2018. Moving target detection and tracking based on pyramid Lucas-Kanade optical flow. IEEE 3rd Int Conf on Image, Vision and Computing, p.66-69. https://doi.org/10.1109/ICIVC.2018.8492786

Wang ZR, Sun X, Diao W, et al., 2019. Ground moving target indication based on optical flow in single-channel SAR. *IEEE Geosci Remote Sens Lett*, 16(7):1051-1055. https://doi.org/10.1109/LGRS.2019.2892488

Wang ZY, Guo W, Sun ZY, et al., 2007. Demonstration of a task-flow based aircraft collaborative design application in optical grid. Proc 33rd European Conf and Exhibition of Optical Communication, p.1-2. https://doi.org/10.1049/ic:20070188

Xu JT, Yang Z, Gao ZY, et al., 2019. A method of biomimetic visual perception and image reconstruction based on pulse sequence of events. *IEEE Sens J*, 19(3):1008-1018. https://doi.org/10.1109/JSEN.2018.2880748

Zhang CX, Chen Z, Li M, 2015. Linear model for 3D motion estimation and shape reconstruction based on the straight-line optical flow. Proc 12th IEEE Int Conf on Electronic Measurement & Instruments, p.1172-1177. https://doi.org/10.1109/ICEMI.2015.7494462

Zhu AZ, Yuan LZ, Chaney K, et al., 2018. EV-FlowNet: self-supervised optical flow estimation for event-based cameras. Proc 14th Conf on Robotics-Science and Systems, p.1-9. https://doi.org/10.15607/RSS.2018.XIV.062

Zhu AZ, Yuan LZ, Chaney K, et al., 2019. Live demonstration: unsupervised event-based learning of optical flow, depth and egomotion. IEEE/CVF Conf on Computer Vision and Pattern Recognition Workshops, p.1694. https://doi.org/10.1109/CVPRW.2019.00216